Biosynthetic Pathways

DOI: 10.1002/anie.201307989

Biosynthesis of Streptolidine Involved Two Unexpected Intermediates Produced by a Dihydroxylase and a Cyclase through Unusual Mechanisms**

*Chin-Yuan Chang, Syue-Yi Lyu, Yu-Chen Liu, Ning-Shian Hsu, Chih-Chung Wu, Cheng-Fong Tang, Kuan-Hung Lin, Jin-Yuan Ho, Chang-Jer Wu, Ming-Daw Tsai, and Tsung-Lin Li**

Abstract: *Streptothricin-F (STT-F), one of the early-discovered antibiotics, consists of three components, a β-lysine homopolymer, an aminosugar* D*-gulosamine, and an unusual bicyclic streptolidine. The biosynthesis of streptolidine is a long-lasting but unresolved puzzle. Herein, a combination of genetic/biochemical/structural approaches was used to unravel this problem. The STT gene cluster was first sequenced from a Streptomyces variant BCRC 12163, wherein two gene products OrfP and OrfR were characterized in vitro to be a dihydroxylase and a cyclase, respectively. Thirteen high-resolution crystal structures for both enzymes in different reaction intermediate states were snapshotted to help elucidate their catalytic mechanisms. OrfP catalyzes an* Fe^{II}*-dependent double hydroxylation reaction converting* L*-Arg into (3R,4R)-*$(OH)_2$*-*L*-Arg via (3S)-OH-*L*-Arg, while OrfR catalyzes an unusual PLP-dependent elimination/addition reaction cyclizing (3R,4R)-*$(OH)_2$*-*L*-Arg to the six-membered (4R)-OH-capreomycidine. The biosynthetic mystery finally comes to light as the latter product was incorporation into STT-F by a feeding experiment.*

Streptothricin F (STT-F), first isolated from *Streptomyces lavendulae* in 1943,[1] is a member of aminoglycoside antibiotics possessing broad-spectrum antimicrobial activities effective against several Gram-positive and Gram-negative bacteria and fungi. STT-F was determined to block the entry of tRNA into the prokaryotic 30S ribosomal subunit, thus resulting in disruption of protein synthesis.[2] STT-F is composed of three components, a carbamoylated D-gulosamine, a β-lysine homopolymer, and an unusual bicyclic amino acid streptolidine (Figure 1a).[3] Formation of the β-lysine homopolymer has recently been elucidated,[4] while that of streptolidine remains an unresolved conundrum. The absolute configuration of streptolidine was determined by King et al.[6] Previous feeding studies have determined that L-arginine (L-Arg) is the starting reactant in the biosynthesis of streptolidine.[5] It would be nice to know what the identity of the proposed intermediates which failed to be converted into streptolidine.[5,7]

To understand streptolidine biosynthesis in STT-F, we set out to sequence the biosynthetic gene cluster of STT-F of the *S. lavendulae* variant BCRC 12163. The biosynthetic gene cluster of STT-F spans approximately 35 kbp and includes 25 putative open reading frames in line with some revealed partial genes or gene clusters (see Figure S1 in the Supporting Information).[4,8] In our gene cluster *orfP* and *orfR* are analogous to *vioC* and *vioD* (42.5% and 40.2% sequence similarities, respectively), which have been determined to be involved in the synthesis of capreomycidine in viomycin.[9]

Both *orfP* and *orfR* were subcloned and expressed in *E. coli* and purified to homogeneity (see Figure S2). For OrfP, typical nonheme iron oxygenase reactions of L-Arg were examined. Four new peaks (**1**–**4**) were observed on the LC/MS trace, where **1** was the major product ($[M+H]^+$: 440.17) and the compounds **2**–**4** were the minor products ($[M+H]^+$: 424.20; Figure 2a; see Figure S3). These products were separated/collected and subjected to NMR analysis. The compounds **1**, **2**, **3**, and **4** were determined to be (3*R*,4*R*)-$(OH)_2$-L-Arg, (4*S*)-OH-L-Arg, (3*R*)-OH-L-Arg, and (3*S*)-OH-L-Arg, respectively (Figure 2B; and Figures S13–16). Reactions were further performed in $^{18}O_2$ or $H_2{}^{18}O$, wherein β,γ-$[^{18}OH]_2$-L-Arg ($[M+H]^+$: 444.24) was exclusively observed under the $^{18}O_2$ conditions, thus concluding that OrfP is an oxygenase which promotes a double hydroxylation of L-Arg at its β- and γ-positions (Figure 3a). The overall Michaelis constant (K_m) and turnover rate (k_{cat}) of OrfP against L-Arg were determined to be (0.689 ± 0.047) mM and (0.402 ± 0.042) s^{-1}, respectively. Interestingly, the substrate is not limited to L-Arg, as D-Arg, L-homoArg, L-canavanine, L-Lys, and L-His can also be hydroxylated to different degrees by OrfP (see Figure S4).

[*] Dr. C. Y. Chang, S. Y. Lyu, Dr. Y. C. Liu, N. S. Hsu, Dr. C. C. Wu, Dr. C. F. Tang, K. H. Lin, Dr. T. L. Li
Genomics Research Center, Academia Sinica
128 Academia Road, Section 2, Nankang, Taipei 115 (Taiwan)
E-mail: tlli@gate.sinica.edu.tw
Dr. J. Y. Ho, Dr. M. D. Tsai
Institute of Biological Chemistry, Academia Sinica
128 Academia Road, Section 2, Nankang, Taipei 115 (Taiwan)
Dr. C. J. Wu
Department of Food Science, National Taiwan Ocean University
2 Pei-Ning Road, Keeling 20224 (Taiwan)
Dr. T. L. Li
Biotechnology Center, National Chung Hsing University
250 Kuo Kuang Road, Taichung 402 (Taiwan)

[**] This research was supported by the National Science Council (NSC) of Taiwan (grants 100-2311-B-001-018-MY3, and 102-2311-B-001-028-MY3 to T.L.L.) and the Academia Sinica intramural funding. Parts of this research were carried out at the National Synchrotron Radiation Research Center (NSRRC), Taiwan. We thank NSRRC and Spring-8 (Japan) for beam time allocations.

Supporting information for this article is available on the WWW under http://dx.doi.org/10.1002/anie.201307989.

 © 2014 Wiley-VCH Verlag GmbH & Co. KGaA, Weinheim

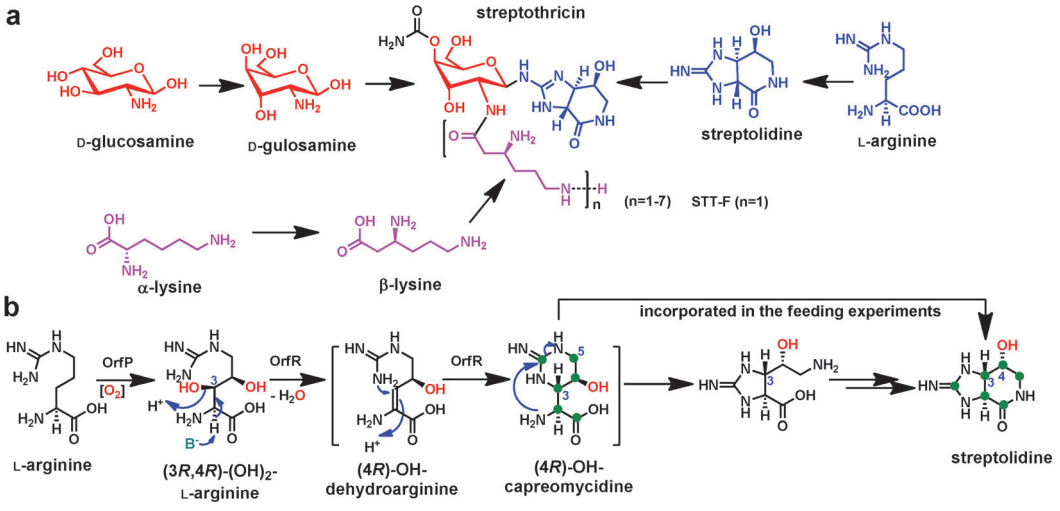

Figure 1. a) Chemical structures and biosynthesis of STT-F. b) Proposed enzyme reactions and feeding results for biosynthesis of streptolidine described in this study (green round dots stand for [^{13}C] enrichment).

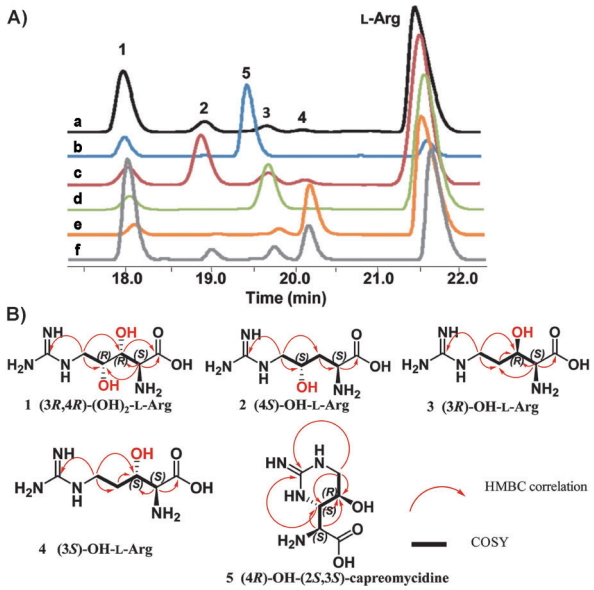

Figure 2. A) HPLC traces of reactions in the presence of OrfP (a), OrfP + OrfR (b), OrfP Q142L/Y257D (c), OrfP D255E (d), OrfP D157A (e), OrfP D157A with L-Arg and WT with [^{13}C$_6$]-L-Arg in stages (see text) (f). B) Structures of compounds **1**–**5**, in which the stereochemistry was determined by NOESY and X-ray crystallography (see Figures S18 and S19).

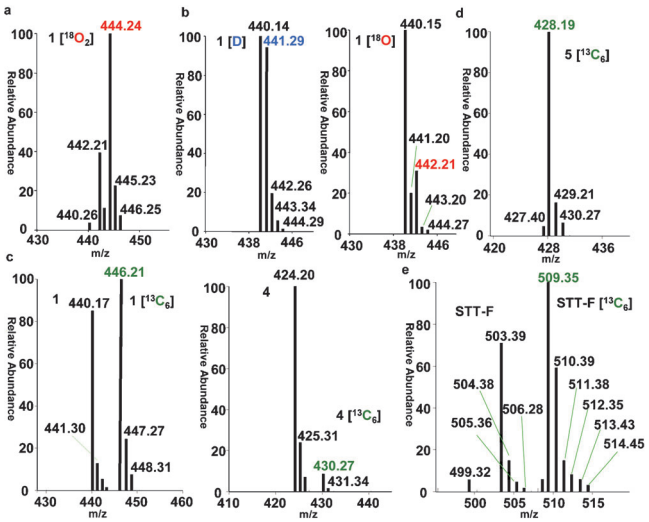

Figure 3. Mass spectrometric analyses. a) Spectrum of [^{18}O$_2$]-**1**. The product was obtained from the OrfP reaction conducted under $^{18}O_2$. b) Spectra of isotope-enriched **1**. The reactions were performed using OrfR E15A in either a D_2O or $H_2{}^{18}O$ buffer solution containing **1**. c) Spectra of **1** and **4**. In terms of yield, the labeled one is greater and less than the unlabeled for **1** (left) and **4** (right), respectively. d) Spectrum of [^{13}C$_6$]-**5**. e) Spectrum of STT-F extracted from the feeding experiment.

We went on to examine the activity of OrfR by comparing the products of the reaction of L-Arg with OrfP and OrfR together (Figure 2A, trace b) with those of OrfP alone (trace a). A new product, **5**, was formed and was characterized by MS and NMR spectroscopy to be dansylated 4-OH-capreomycidine ([*M*+H]$^+$: 422.28; Figure 2b; see Figures S3 and S17). Its configuration was further determined by 2D NOESY correlation to be (4*R*)-OH-(2*S*,3*S*)-capreomycidine (see Figures S17 and S18). The compounds **2**-**4**, and single hydroxylation analogues of D-Arg, L-homoArg, L-canavanine, L-Lys, and L-His are not substrates of OrfR, thus suggesting the cyclase is highly specific. The Michaelis constant (K_m) and turnover rate (k_{cat}) of OrfR against (3*R*,4*R*)-(OH)$_2$-L-Arg were determined to be (0.183 ± 0.002) mM and (0.952 ± 0.007) s^{-1}, respectively.

Particular attention was paid to the reaction order because of the stereocontrol and the ring cyclization. Ten high-resolution protein crystal structures of OrfP in free enzyme, binary, ternary, and quaternary complexes were solved at a 1.7–2.6 Å resolution using the structure of VioC (PDB code: 2WBO) as a model.[10] Data processing and refinement statistics are summarized in Table S1. Superposition of free and complexed OrfP structures revealed a substantial conformational change, thus suggesting that a flaplike domain (L198–L242) on the top of the β-barrel adopts two structural modes (see Figure S5). The open form allows substrates to enter the active site, and the closed form enables formation of the reactive oxygen species. In light of the free OrfP structure, three residues, His154, Glu156, and His303, buried in the middle of the β-barrel, organize an ideal geometry to chelate a metal ion (see Figure S6a). A chunk of

 © 2014 Wiley-VCH Verlag GmbH & Co. KGaA, Weinheim

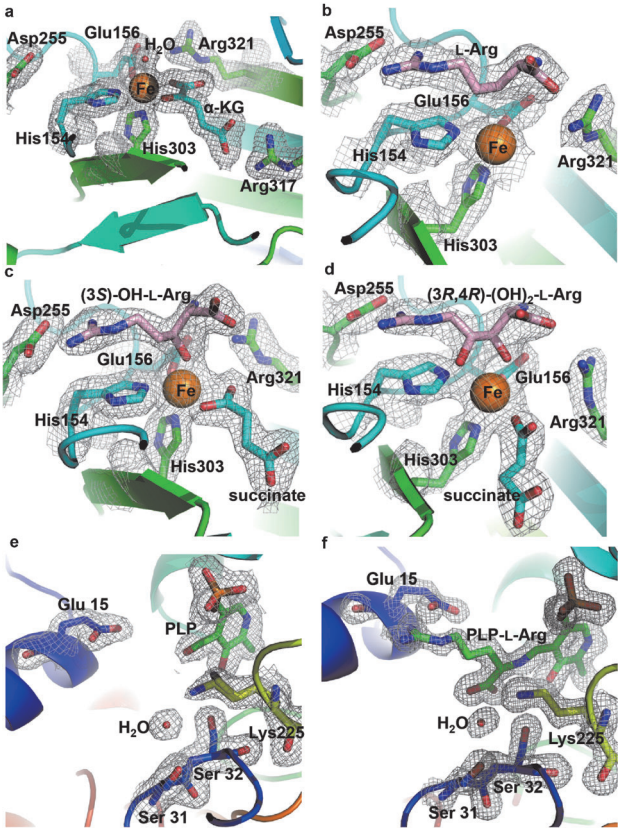

Figure 4. The active sites of a) OrfP·Fe·α-KG, b) OrfP·Fe·L-Arg, c) OrfP·Fe·succinate·(3*S*)-OH-L-Arg, d) OrfP·Fe·succinate·(3*R*,4*R*)-$(OH)_2$-L-Arg, e) OrfR·PLP, f) OrfR·PLP·L-Arg. The 2 F_o-F_c electron density maps are contoured at 1 σ.

round density situated in the center of the facial triad in the binary structure (OrfP·Fe) is likely a metal ion (Figure S6b). The attribute of the density was determined to be a ferric ion by X-ray absorption spectroscopy (XAS; Figure S7). In the structure of OrfP·Fe·α-KG, the α-KG along with the facial triad and a water molecule result in a tetragonal bipyramidal structure, wherein the imidazole Nε2 of His^{154}, the carboxy anion of Glu^{156}, and the α-ketoacid moiety of α-KG span the equatorial plane with the imidazole Nε2 of His^{303} and a water molecule each perched atop both sides of the equatorial plane (Figure 4a). In addition to the interaction between the α-ketoacid bidentate and iron, α-KG also associates with Arg^{317} through an electrostatic interaction (Figure S8a). In the structure of OrfP·Fe·L-Arg, L-Arg takes an S conformation with its carboxy and guanidino groups electrostatically interacting with Arg^{321} and Asp^{255}, respectively (Figure 4b, and Figure S8b). L-Arg anchors on the top of the sixth coordinate with the pro-*S* H atom of the β-carbon atom in close contact with the iron center. A quaternary structure was further obtained, wherein α-KG is superseded by succinate, a decarboxylated product of α-KG. Surprisingly, L-Arg has been transformed into (3*S*)-OH-L-Arg with the β-OH group taking the sixth coordinate, thus suggesting a hydrogen abstraction/oxygen rebound mechanism (Figure 4c). Most strikingly, in the structure of OrfP in complex with (3*R*,4*R*)-$(OH)_2$-L-Arg, the product adapts a thermodynamically disfavored eclipsed conformation (Figure 4d). The β,γ-vicinal diol chelates the iron center with γ-OH taking the sixth coordinate, thus suggesting that the adjacent β-OH group plays critical roles in the control of both the regio- and stereoselectivity. To this end, the solved OrfP structures provide detailed molecular snapshots, thus enabling one to visualize almost every step in the biochemical transformation.

Next, we performed alanine-scanning site-directed mutagenesis to validate the above observations. The substitution of either of the facial triad residues His^{154}, Glu^{156}, or His^{303} with Ala, not surprisingly, abolished the enzyme activity. Replacing either of the substrate-binding residues Asp^{255}, Arg^{321} (for L-Arg), and Arg^{317} (for α-KG) with Ala also showed no enzyme activity (Figure S8), thus confirming the given functions. Interestingly, the double mutant Q142L/Y257D catalyzes formation of **2**, while the single mutants D255E and D157A mainly produce **3** and **4**, respectively (Figure 2a). The possible roles for these selected residues in regio- and stereoselectivity are described in Figure S9. Biochemical assays further revealed that only **2** and **4** could be transformed into **1**, thus indicating that OrfP has some flexibility in the reaction order, while the stereochemistry is highly specific.

To our knowledge the stereospecific vicinal dihydroxylation reaction carried out by OrfP is the only example in the nonheme Fe^{II} α-KG-dependent oxygenase family.[11] As **1**–**4** were identified, the radical mechanism is favored. Taken together, the overall catalytic mechanism of OrfP is summarized as follows (Figure 5A): a) Fe^{III} is first reduced to Fe^{II} under physiological conditions. α-KG then comes in to form a tetragonal bipyramidal coordination with a water molecule atop the plane. b) When L-Arg enters its binding site, O_2 could supersede H_2O to form a Fe^{II}-superoxide anion or a Fe^{III}-superoxide. c) The superoxide then readily attacks the carbonyl carbon atom of a α-KG, thus resulting in succinic acid (by decarboxylation) and the reactive Fe^{IV}-oxo species (by heterolysis). d) Fe^{IV}-oxo abstracts the pro-*S* H atom from the β-carbon atom of L-Arg to form Fe^{III}-OH and the corresponding radicals. e) (3*S*)-OH-L-Arg (**4**) is formed by the rebound recombination of the resulting carbon radical and the iron-bound hydroxyl. f) **4** re-engages in the reaction, then g) it restructures with the pro-*R* H atom of the γ-carbon atom exposed to the iron center. h) (3*R*,4*R*)-$(OH)_2$-L-Arg (**1**) is formed under the same reaction course.

The initial phase of OrfR was resolved by using the method of single-wavelength anomalous diffraction (SAD) on heavy-atom (Au) derivatized crystals. An asymmetric unit contains a single polypeptide chain (Figure S6c), while a crystallographic twofold axis generates a dimer. Consistently, AUC analysis suggests that OrfR is a dimer in solution (see Figures S2b and S10). Two additional OrfR structures were obtained, thus including binary (OrfR·PLP) and ternary (OrfR·PLP·L-Arg; Figures 4e,f) complexes. The (3*R*,4*R*)-$(OH)_2$-L-Arg-complexed ternary structure was not obtained. Soaking the binary crystals with L-Arg was then attempted in a bid to get an intermediate state. The OrfR·PLP·L-Arg ternary structure was finally acquired, wherein the PLP aldehyde group forms an aldimine linkage with the α-amino group of L-Arg. (Figure 4f). For the PLP-dependent six-membered-ring cyclization reaction, a general base to

 © 2014 Wiley-VCH Verlag GmbH & Co. KGaA, Weinheim

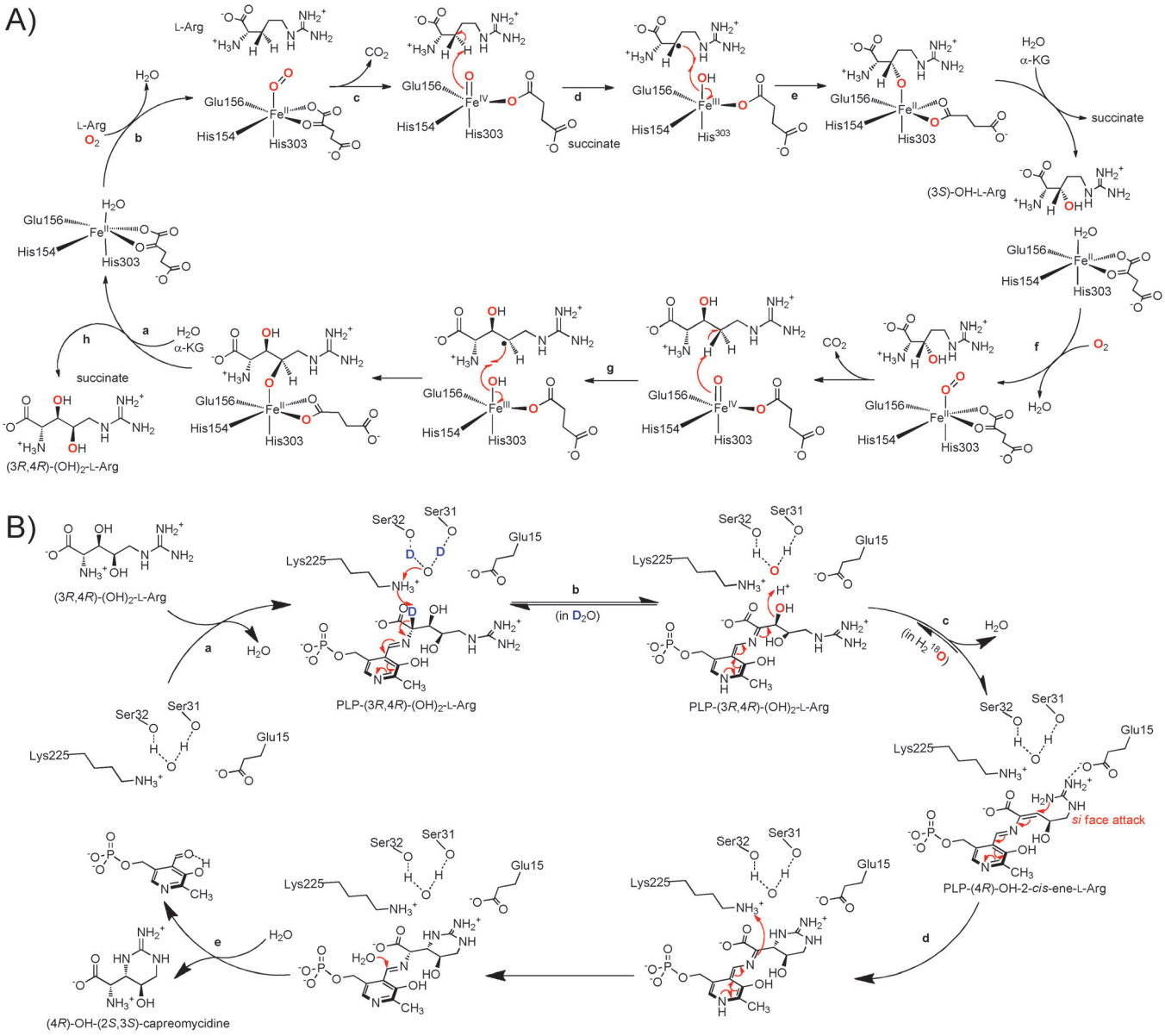

Figure 5. a) The proposed double hydroxylation mechanism carried out in OrfP. b) The proposed six-membered-ring cyclization mechanism carried out in OrfR.

deprotonate the α-carbon atom of L-Arg is often necessary.[9a,c] Lys225, which lies close to the aldimine moiety of the PLP-L-Arg complex, is likely to assume the function of the general base. This role of Lys225 is supported by the fact that a K225A mutation renders the enzyme inactive. Additionally, a water molecule, which is held by the residues Ser31 and Ser32 within a short distance of Lys225, was identified in both structures (Figure 4e,f). The water-assisted deprotonation may be beneficial in lowering the pK_a value of Lys225 to enable its activity as a general base. Biochemical assays support this hypothesis as the enzyme activity plunged to 8.5% when a double mutant (S31A/S32A) was examined. To determine if the reaction follows the elimination/addition mechanism, an isotope-labeling experiment was performed: Enzymatic reactions using the mutant E15A with **1** (OrfP product) were conducted in either a D_2O or $H_2{}^{18}O$ buffer solution and then subjected to mass spectrometry analysis in due course. The mass analysis revealed that the mass units of the compound increased by 1 or 2 a.m.u. in both D_2O and $H_2{}^{18}O$ (Figure 3b). We reasoned that the proton at the α-carbon atom of **1** undergoes a deprotonation/reprotonation reaction, and that the deprotonation could promote a dehydration/rehydration reaction in the PLP conjugation system. Because of the unavailability of the OrfP·PLP·(4*R*)-OH-dehydroarginine complex, two possible dehydrated intermediates, (4*R*)-OH-2-*cis*/*trans*-ene-L-Arg, were modeled in OrfR (see Figure S11). The *cis* conformer is favored, as the carboxy group of Glu15 is likely in close proximity to the guanidinium group of **1**, and would enable the terminal amine to be a better nucleophile, as well as lead to a configurationally

 © 2014 Wiley-VCH Verlag GmbH & Co. KGaA, Weinheim

correct conformer. The fact that the E15A variant is inactive supports this reasoning. In contrast, the *trans* conformer is not favored because of considerable steric hindrance. OrfR is very specific to the substrate, as monohydroxy D/L-Arg, L-His, or L-Lys, hydroxy canavanine, or dihydroxy homoArg (Figure S4) cannot be cyclized. This result underscores that the γ-hydroxy group is critical in the formation of the correct conformer.

The OrfR-catalyzed cyclization reaction is summarized as follows (Figure 5B): a) **1** first binds to its binding site and reacts with PLP to form an aldimine adduct. b) The active-site Lys225, assisted by the Ser31-Ser32 pair, removes the α-C proton of the substrate. c) The resulting α-C anion delocalizes into the PLP conjugation system to facilitate an α,β-elimination for the formation of a coplanar PLP-(4*R*)-OH-2-*cis*-ene-Arg adduct. d) The adduct adopts a conformation with the guanidino group resting right above the *si* face of β-carbon atom; the terminal amine may be localized by Glu15 to trigger the conjugate addition for the formation of a six-membered species. e) Finally, a water molecule enters and hydrolyses the aldimine linkage to free PLP and (4*R*)-OH-(2*S*,3*S*)-capreomycidine.

The revelation of the two unexpected products seems to have answered why isotope-labeled **4** and (2*S*,3*S*)-capreomycidine failed to be incorporated into STT-F in previous feeding experiments. That is, they are not the authentic intermediates in the biosynthesis of streptolidine. However, it still remains controversial, because **4** appears to be the intermediate of OrfP despite having low yield (Figure 2A, trace a). To solve this contradiction, we took advantage of the mutant D157A to generate a considerable amount of **4** (Figure 2A, trace e).[$^{13}C_6$]-L-Arg (equal quantity to L-Arg) was then added into the solution and supplemented with OrfP WT in place of the mutant which was filtered out beforehand. Both the LC traces and the isotope profiles confirm that the conversion of **4** into **1** is low (Figure 2A, traces a and f); Figure 3c), thus suggesting that **4** is a leaky product and that L-Arg most likely undergoes two sequential hydroxylation reactions to give **1** in OrfP before release (Figure 5a).To conclude our finding, we further performed a feeding experiment by adding [$^{13}C_6$]-**5** into the growing medium of *S. lavendulae* variant BCRC 12163. STT-F secreted in the broth was recovered and subjected to mass analysis, whereby the molecular mass of STT-F clearly shows an additional six mass units in the mass spectrum, thus answering the long-lasting biosynthetic conundrum of streptolidine (Figure 1b, and Figures 3d and e).

Our demonstration of the stereo- and regiospecific double hydroxylation reaction makes OrfP unique in the α-KG-dependent enzyme family. In addition, our demonstration that OrfR executes sequential α,β-elimination (dehydration) and conjugate addition (cyclization) reactions makes it a new subclass in the PLP-dependent enzyme family, thus adding to the vast variety of reactions, such as transamination, racemization, decarboxylation, and elimination.[12] Additionally, dozens of new STT-F analogues have recently been discovered, and showed substantial biological activities against flocks of bacteria, viruses, and lines of cancer cells,[13] thus indicating important roles of streptolidine in antimicrobial/anticancer activity. The structural and biochemical information garnered here may provide a shortcut to making new capreomycidin/strpeptolidine analogues for various medicinal purposes.

Experimental Section

Protein expression, purification, and biochemical assays were performed according to standard protocols. Molecular replacement (MR) and single-wavelength anomalous dispersion (SAD) methods were used to solve native and complexed structures of OrfP and OrfR. Mutants were made using QuikChange. Biochemical analysis for wild type enzymes and mutants were performed using LC-MS. The small compounds of enzymatic products were collected by LC and identified by NMR spectrosocopy. Structure dynamics were determined by analytical ultracentrifugation (AUC).

Accession codes: The STT-F biosynthetic gene cluster from *Streptomyces lavendulae* variant BCRC 12163 has been deposited in the GeneBank under accession numbers KF498701. The coordinates have been deposited in the Protein Data Bank under accession numbers 4M23 (Free OrfP), 4M2I (OrfP·Fe), 4M25 (OrfP·Fe·α-KG), 4M27 (OrfP·Fe·L-Arg), 4M2C (OrfP·Fe·D-Arg), 4M2E (OrfP·Fe·L-homoArg), 4M2F (OrfP·Fe·L-canavanine), 4M26 (OrfP·Fe·succinate·(3*S*)-OH-L-Arg), 4M2G (OrfP·Fe·succinate·(3*R*,4*R*)-$(OH)_2$-L-Arg), 4NE0 (OrfP·D157A·Fe·succinate·(3*S*)-OH-L-Arg), 4M2J (OrfR·PLP·Au), 4M2K (OrfR·PLP), and 4M2M (OrfR·PLP-L-Arg).

Received: September 11, 2013
Revised: October 30, 2013
Published online: January 21, 2014

Keywords: biosynthesis · enzymes · isotopic labeling · protein structures · reaction mechanisms

[1] S. A. Waksman, *J. Bacteriol.* **1943**, *46*, 299–310.
[2] a) I. Haupt, R. Hubener, H. Thrum, *J. Antibiot.* **1978**, *31*, 1137–1142; b) I. Haupt, J. Jonak, I. Rychlik, H. Thrum, *J. Antibiot.* **1980**, *33*, 636–641; c) A. L. Goldstein, J. H. McCusker, *Yeast* **1999**, *15*, 1541–1553; d) P. Hentges, B. Van Driessche, L. Tafforeau, J. Vandenhaute, A. M. Carr, *Yeast* **2005**, *22*, 1013–1019; e) J. Shen, W. Guo, J. R. Kohler, *Infect. Immun.* **2005**, *73*, 1239–1242; f) A. Idnurm, J. L. Reedy, J. C. Nussbaum, J. Heitman, *Eukaryotic Cell* **2004**, *3*, 420–429; g) P. B. Joshi, J. R. Webb, J. E. Davies, W. R. McMaster, *Gene* **1995**, *156*, 145–149.
[3] a) H. E. Carter, E. E. Vantamelen, J. R. Dyer, E. E. Daniels, C. C. Sweeley, C. A. West, C. P. Schaffner, H. A. Whaley, J. E. Mcnary, *J. Am. Chem. Soc.* **1961**, *83*, 4296; b) S. Kusumoto, Y. Kambayashi, S. Imaoka, K. Shima, T. Shiba, *J. Antibiot.* **1982**, *35*, 925–927.
[4] C. Maruyama, J. Toyoda, Y. Kato, M. Izumikawa, M. Takagi, K. Shin-Ya, H. Katano, T. Utagawa, Y. Hamano, *Nat. Chem. Biol.* **2012**, *8*, 791–797.
[5] a) S. J. Gould, J. N. Lee, J. Wityak, *Bioorg. Chem.* **1991**, *20*, 333–350; b) S. J. Gould, K. J. Martinkus, C. H. Tann, *J. Am. Chem. Soc.* **1981**, *103*, 2871–2872; c) S. J. Gould, K. J. Martinkus, C. H. Tann, *J. Am. Chem. Soc.* **1981**, *103*, 4639–4640; d) K. J. Martinkus, C. H. Tann, S. J. Gould, *Tetrahedron* **1983**, *39*, 3493–3505.
[6] B. W. Bycroft, T. J. King, *J. Chem. Soc. Chem. Commun.* **1972**, 652.
[7] a) S. J. Gould, T. K. Thiruvengadam, *J. Am. Chem. Soc.* **1981**, *103*, 6752–6754; b) T. K. Thiruvengadam, S. J. Gould, D. J. Aberhart, H. J. Lin, *J. Am. Chem. Soc.* **1983**, *105*, 5470–5476; c) V. A. Palaniswamy, S. J. Gould, *J. Chem. Soc. Perkin Trans.*

 © 2014 Wiley-VCH Verlag GmbH & Co. KGaA, Weinheim

1 **1988**, 2283 – 2286; d) M. D. Jackson, S. J. Gould, T. M. Zabriskie, *J. Org. Chem.* **2002**, *67*, 2934 – 2941.
[8] a) M. A. Fernandez Moreno, C. Vallin, F. Malpartida, *J. Bacteriol.* **1997**, *179*, 6929 – 6936; b) J. Li, Z. Guo, W. Huang, X. Meng, G. Ai, G. Tang, Y. Chen, *Sci. China Ser. C* **2013**, *56*, 619 – 627.
[9] a) X. Yin, K. L. McPhail, K. J. Kim, T. M. Zabriskie, *ChemBioChem* **2004**, *5*, 1278 – 1281; b) X. Yin, T. M. Zabriskie, *ChemBioChem* **2004**, *5*, 1274 – 1277; c) J. Ju, S. G. Ozanick, B. Shen, M. G. Thomas, *ChemBioChem* **2004**, *5*, 1281 – 1285.
[10] V. Helmetag, S. A. Samel, M. G. Thomas, M. A. Marahiel, L. O. Essen, *FEBS J.* **2009**, *276*, 3669 – 3682.
[11] a) M. J. Ryle, R. P. Hausinger, *Curr. Opin. Chem. Biol.* **2002**, *6*, 193 – 201; b) E. G. Kovaleva, J. D. Lipscomb, *Nat. Chem. Biol.* **2008**, *4*, 186 – 193.
[12] a) E. F. Oliveira, N. M. Cerqueira, P. A. Fernandes, M. J. Ramos, *J. Am. Chem. Soc.* **2011**, *133*, 15496 – 15505; b) A. C. Eliot, J. F. Kirsch, *Annu. Rev. Biochem.* **2004**, *73*, 383 – 415.
[13] a) M. Gan, X. Zheng, L. Gan, Y. Guan, X. Hao, Y. Liu, S. Si, Y. Zhang, L. Yu, C. Xiao, *J. Nat. Prod.* **2011**, *74*, 1142 – 1147; b) W. E. Brown, J. Szanto, E. Meyers, T. Kawamura, K. Arima, *J. Antibiot.* **1977**, *30*, 886 – 889; c) M. Gan, X. Zheng, Y. Liu, Y. Guan, C. Xiao, *Bioorg. Med. Chem. Lett.* **2012**, *22*, 6151 – 6154.

 © 2014 Wiley-VCH Verlag GmbH & Co. KGaA, Weinheim